Oxygen nightglow vertical distribution from the VIRTIS Near IR observations in the Venus upper atmosphere

G. Piccioni[(1)], L. Zasova[(2)], A. Migliorini[(1)], P. Drossart[(3)], A. Shakun[(2)], A. García Muñoz[(4)], F. P. Mills[(4)], A. Cardesin[(1)] and the VIRTIS-Venus Express Team

[(1)] INAF-IASF Rome, Italy
[(2)] Space Research Institute of Russian Academy of Science (IKI), Moscow, Russia
[(3)] Obs. of Meudon, Paris, France
[(4)] Research School of Physical Sciences and Engineering, The Australian National University, Canberra, ACT 0200, Australia

Abstract

The oxygen nightglow at Venus has been intensively studied from ground observations since its discovery in spectra obtained on 1975 (Connes et al, 1979) during the inferior conjunction periods, with some glimpses from space during the flybys of the Galileo (NIMS) mission.
Here we discuss the vertical profile of the oxygen nightglow in limb view geometry as observed by VIRTIS, emphasizing the vertical transport more than the horizontal motion which is more extensively studied in another paper of this issue (Hueso et al, 2008). We will also show some results coming from nadir observation geometry, providing an extended view of how the vertical transport is locally distributed. Both the (0-0) band at 1.27 μm and the (0-1) band at 1.58 μm are detected and a ratio of transition probabilities $A_{00}/A_{01} = 63\pm6$ is inferred.
We have analyzed up to now 31 cubes for 13 orbits, covering latitude range from 10 to 75° N. The vertical distribution of the O_2 emissions are very similar and their peak is typically found to

be at 98±2 km with some exceptions. Cases where the peak is significantly higher in altitude, at about 103 km, are present and other cases with a double peak exist as well. No obvious geographical dependence has been found for the peak altitude and emission strength in long term (days or weeks), while more regular trends versus local time or latitude are observed in a short term within the same orbit.

Introduction

The $O_2(^1\Delta \rightarrow {}^3\Sigma)$ infrared airglow on Venus was discovered from the ground using a Fourier transform spectrometer (Connes et al., 1979) and it showed comparable brightnesses on both the day and the night sides with corrected vertically integrated emission of 1.2-1.5 Mega-Rayleighs (MR). Since then it has been intensively observed on multiple ground observations campaign (Crisp et al., 1996, Othsuki et al. 2005) during inferior conjunction periods. The nightglow oxygen emission is very important to constraint the photochemical model and it is an effective tracer to study the upper atmospheric circulation on Venus. The O_2 airglow on the night side of Venus is produced after recombination of O atoms, which are the result of the CO_2 photolysis on the day side. A major fraction of these oxygen atoms (J-C Gerard et al., 2008) is then transported to the night side via the Sub-Solar to Anti-Solar (SS-AS) circulation in the 90-130 km range of the lower thermosphere (Bougher and Borucki, 1994). Once on the nightside the O atoms can recombine in the three body recombination reaction O + O + M --> O_2^* + M, with O_2^* being the excited state of molecular oxygen. The net yield for production of the $O_2(a)$ state after multiple collisions of the upper excited states has been estimated to be between 0.65-0.75 (Crisp et al. 1996). The Venus Express mission and in particular its VIRTIS (Visible and Infrared Thermal Imaging Spectrometer) instrument on board (Piccioni et al., in press, Drossart et al. 2007), gave us the opportunity to regularly study the oxygen airglow in nadir geometry and, in addition, to perform for the first time direct measurements of its vertical profile by using the peculiar limb view geometry, only possible from an orbiting spacecraft around it. The first results of the oxygen nightglow have already been recently published (Drossart et al., Nature 2007). The emission is known to show very fast variations of its intensity and local distribution over time scales of hours. Despite this, it has been recently shown from the VIRTIS data in nadir geometry that in a long term average it provides almost firm ideal picture of the SS-AS circulation with a maximum in the region of the AS point at about midnight (J-C Gerard et al., 2008). Thermal emission from the lower atmosphere leaks through a window in the CO_2 absorption spectrum and appears only partly attenuated at the altitudes of emission of the (0-0) O_2 IR atmospheric band. In limb geometry at an altitude above 90km, the thermal emission is negligible and the oxygen emission appears unblended. In nadir geometry the two emissions cannot spectrally separated at the resolving power of VIRTIS, which is about 130 at this wavelength. Fortunately the spectral peak of the O_2 emission does not coincide with the thermal emission peak, the latter appearing at a somewhat longer wavelength. This enables us to separate the O_2 emission areas visually by color (see fig. 1c). In the case of limb observations the input of thermal emission may be usually ignored comparing to the O_2 emission in spite of the presence of faint scattering haze at high altitudes significantly decreasing above 90 km. In cases of nadir observations the thermal emission can't be considered negligible and the oxygen nightglow emission can be corrected for the thermal part empirically by using the radiance at 1.18 um rescaled by a factor from 0.27 to 0.38 evaluated time to time from the considered observations.

Observations geometry

There are two types of observation geometry with VIRTIS-M: limb and nadir modes. The view in the nadir mode allows to get an extended coverage of the atmosphere far away in the orbit of the spacecraft. The limb mode permits direct access to the emission vertical profile. Another advantage of the limb mode is that the integrated emission volume is about 50 times larger than in nadir mode, so that faint emissions are more favorably seen. The polar orbit of Venus Express with the pericenter at about 75° N makes it possible to conduct frequent limb observations in the northern hemisphere. This is in order to limit the slant distance to be shorter than 15 000 km such that the vertical spatial resolution would be about 2.5 km with the VIRTIS Instantaneous Field of View (IFOV). Further more shorter slant distances are difficult to achieve due to the high relative speed of the instrument line of sight with respect to the Venus limb.

The current limb pointing is executed through an inertial attitude of the spacecraft (SPC) and the limb is scanned by its +Z axis, about aligned with the instrument FOV, during its motion around Venus.

The VIRTIS-M slit, orthogonal to the +Z axis and parallel to the +Y axis along the solar panels, can be oriented about parallel or normal to the limb respectively in the “in plane” or “tangential” limb types. This nomenclature which seems in contradiction with the actual orientation of the VIRTIS slit is due to the complementary orientation of the VIRTIS and SPICAV slits. The limb pointing is indeed managed by the SPICAV instrument and the orientation is referred to SPICAV. The tangential limb mode provides the best altitude coverage of the limb because the slit spans the full vertical extension in one shot and different samples along the slit cover the limb at different places, extending the horizontal spatial coverage (Titov, et al., 2006).

Many observations have been obtained in this mode, usually covering the northern hemisphere from the equatorial region up to about 70-75° N. Examples of observations in this mode are shown in Fig. 1 (orbit 76-18 and 317-06-07-08, obtained at higher spatial resolution), where the latitude range from approximately 10 to 75° N is divided in three separate zones.

One of the most interesting examples of observations in plane limb mode is in the orbit 271, session 09 shown in Fig. 1. It covers the low latitudes range from 15 to 35° N.

In future a new limb pointing call “limb tracking” will be tested and used for operations planning. This new mode will allow a longer hold at fix height of the line of sight and it will also improve the vertical spatial sampling by about one order of magnitude when used in combination with a finer scan of the VIRTIS-M scanning mirror.

Limb data selection

As of today, the VIRTIS instrument has performed more than 700 revolutions around the planet, acquiring more than 500 Gigabytes of data in different geometry configurations. For this study we have selected data acquired in the limb configuration for the period February-April 2007 and with at least 8 seconds of exposure time, in order to have high SNR (Signal to Noise Ratio) in the relevant spectral range. With such exposure times, the thermal part of the spectrum over 4 microns is saturated but oxygen emissions in the IR are very well defined. The selected data provide a good vertical spatial resolution of the order of 2 km/pixel.

In table 1 it is shown a summary of the selected data. For each orbit a typical series of 3 consecutive cubes, also called sessions, are available for three different regions of the planet. During the period February-March 2007 (MTP011), all data belonging to the internal category "cases 7" (limb mode in either in plane or tangential) have been acquired at about the same local time, between 00h and 01h, and observed almost at the same latitude.

Each data cube spans about 30 deg in latitude, with the entire dataset covering from 10 to 70 deg N.

Vertical profile of the O2 emission in limb view

The limb observations selected to retrieve the vertical profile are averaged within 5° of latitude and all pixels are processed along the local normal. In the selected column they are then smoothed over 1 km of altitude. A typical result of the process is shown in Fig. 2.

The vertical profile of oxygen airglow is dictated by a competition of the atomic oxygen recombination and the quenching deactivation of CO_2. Both factors depend on the physical conditions of the atmosphere. Collisional and radiative lifetimes are equal at 91 km and at the emission peak approximately 80 % of the O_2 $^1\Delta_g$ molecules deactivate by emitting 1.27 um photons (Gerard et al., 2008).

In our case variability of the limb profiles are noticed and a subset of observations is shown in Fig. 3. Intensity scale of the abscissa is emission rate of oxygen airglow at 1.27 um along the line of sight.

It can be seen that the emission rate around the peak changes by an order of magnitude for different orbits and locations. Peak altitude changes from 96 to 103 km in the considered cases. In many cases the peak intensity decreases with increasing latitude, but this is not a general case and sometimes it is observed an inverse behavior.

Vertical profiles of the volume intensity are retrieved using the ‘onion peeling’ technique (Sharma, et al., 1985) starting from the observed limb profiles. In the retrieval we experienced negative values of intensity below the maximum of emission at 85-90 km. The reason of this negative intensity can be due to an overestimation of the emission from the hypothesis about spherical symmetry of the emitting layer. Constraining the emission to be positive versus altitude we may estimate the upper limit of the horizontal size of the O_2 emitting area. This has been evaluated in the range from 500 to 1500 km for several orbits. From the observed limb profiles, by means of a numerical solution of the inverse problem for the Fredholm integral equation, it is possible to retrieve the volume emission profile, which is in turn the O_2 non-LTE emission profile above 90 km. As an additional product, we get also the thermal radiation profile below 90 km. Below 90 km the thermal emission scattered by clouds in the region at 1.27 um starts to be significant and the vertical profile becomes representative of the vertical profile of the clouds. In Fig. 4 we plot an example of oxygen airglow retrieval and also the normalized radiation profile at 1.74 µm, which is pure thermal radiation from the clouds. Both profiles follow a common trend below 90 km because either the emission at 1.27 and 1.74 um depends more tightly on the thermal emission only.

The profiles shown in Fig. 4 from different orbits and locations give no evidence of an important correlation of the peak altitude versus latitude. However, when single sessions within an orbit are considered, acquired almost simultaneously (a few minutes), the peak altitude of the profiles show regular trends along the latitude or local time. One case of such vertical profiles is shown in Fig. 5 for orbit 317. It can be seen that for this orbit we find a monotonous increase of peak altitude and decrease of peak intensity with increasing latitude. In addition, the Full Width at Half Maximum (FWHM) of the emission changes by a factor of two: from 15-16 to 7-8 km versus latitude; the profile becoming narrower at higher latitudes. The peak altitude depends indirectly on the atmospheric pressure and thus it is reasonable to expect a lower altitude in the anti-solar region where the subsidence is more important. In terms of pressure, the different peak altitude in the horizontal direction is in fact a necessary condition to force the thermospheric circulation whose horizontal winds are driven by the pressure gradient forces at about the altitude level of emission. All of this can explain the more regular altitude profile versus the horizontal direction which is found at short time, more related to the instantaneous dynamics. In general instead no obvious correlation can be found for the peak height because only the instantaneous spatial gradient is significant to force the airglow.

This is better seen in Fig. 6 where it is shown the measured vertical profile of the airglow versus latitude in limb mode for some orbits. In some case the vertical distribution follows a quite regular trend with latitude, meaning that there are favorable conditions for important horizontal winds. More static conditions with somewhat reduced altitude and therefore pressure gradients can indicate more favorable conditions for downwelling rather than horizontal motion.

From a more general point of view, we tried to investigate on which parameter depends the emission rate. At the moment, due to the more limited coverage in terms of local time, usually around midnight ±1h, we focus on a possible dependence from the latitude.

In Fig. 7 we summarize the results from the data set analyzed to date. We find a weak dependence between vertical emission rate (emission referred to the vertical direction) and latitude, see Fig. 7a. A weak dependence is also observed between the vertical emission rate and the peak altitude, see Fig. 7b. The vertical emission rate appears to be increasing when the altitude of the peak increases. Very weak dependence is observed between altitude and latitude, see Fig. 7c. The intensity of the O_2 emission decreases more or less regularly with increasing latitude. In Fig. 7d, isolines of emission rate in coordinates latitude-altitude are shown. The highest intensity of the O_2 emission is observed at low latitudes, when position of the peak is around 100 km and above. These results may not represent the general situation as previously explained and more data have to be analyzed for a possible clearer figure.

From the shape of the measured vertical profiles shown in Fig. 3, we identify two different families. The first one, that we call "standard", is when the vertical profile of the O_2 emission have only one peak at a typical altitude of 97±1 km. The second one is when the vertical profile is wider and double peaked or with a more pronounced peak appearing at higher altitude above 100 km, typically at 104 km. In the second case, along with the peak altitude increase, the O_2 vertical emission rate seems increasing with increasing altitude.

Example of the first kind is in orbit 317 (Fig. 5), while the second one is discussed in the next paragraph.

Detection of double peaked airglow

In many cases a second peak in the vertical airglow profile emission is observed. Some example is shown in Fig. 8, where the measured vertical profiles are shown on the left side and correspondent acquired images of the limbs at 1.27 um are observed in the right side. The net separation of the two layers is clearly visible in the images. The usual peak of emission is observed at about 96-98 km height, while the second one is located at about 103-105 km.

First of all it has to be said that this phenomenon is not an artefact caused by the geometry or some instrumental effect because the “secondary” peak emerges at higher altitude and sometime it is even brighter than the lower peak. There is then no ambiguity due to horizontal homogeneity and its structure is actually vertical. The double peak is more frequently observed at high latitudes, from 45 to 70 deg.

With a “regular” atmosphere there is no reason to have a similar vertical profile therefore a possible explanation is that propagating gravity waves can modulate the atmospheric density, helping the collisions of the oxygen atoms at higher altitudes. Strong wave structures have already been observed by PVO star trackers (Bougher and Borucki, 1994) and they have been thought to be the main modulation which drives form low atmospehere up rapid changes in airglow intensity. The frequency of the double peak emission at the above mentioned latitudes is consistent with the more frequent presence of the gravity waves at higher latitudes.

It must be said that a double peak from the retrieval of the oxygen vertical profile is quite common also when the measured vertical profile is located in a single peak. However this is consistent with the previous assumption of the gravity waves as possible cause because the oxygen yield is estimated from the nightglow emission which mainly depend on the oxygen atoms collision.

Oxygen band ratio

The oxygen on Venus is a very important tracer to study the upper atmosphere. As already state, the most important reservoir of oxygen on Venus is from photolysis of carbon dioxide. Hence, there is a completely different chemistry from Earth's one, which rules over oxygen on Venus. As in the case of the Earth, we can know about different chemical species and physical conditions, by measuring the ratio between the two main oxygen emissions in the NIR, the brighter one $a^1\Delta_g$ at 1.27 µm and the weaker one $X^3\Sigma_g^-$ at 1.58 µm.

We have used the observations in limb view geometry and for each emission, the band integral has been calculated and the continuum contribution has been evaluated. The integral band of the emission at 1.27 μm which is very intense is easy to be quantified. The integral band of the 1.58 um is more difficult to be evaluated due to the fainter signal and the limits must be set by using the HITRAN database (Rothman L.S., et al., 2005**).**

In Fig. 9 the 1.27 μm/1.58 μm oxygen bands ratio is shown for several sessions, represented in the abscissa. The measured weighted mean is 77.9 ± 8.7, which results to 63±6 for the ratio of the transition probabilities A_{00}/A_{01}. The uncertainty is basically due to the difficult evaluation of the tale and continuum of the 1.58 um band. Both bands had been observed in the terrestrial atmosphere, but never simultaneously. In the laboratory, they are quite weak and difficult to be measured. The most recent reference for the A_{01} band is in Campargue et al. 2005. After correction of a mistake in their conversion from absorption strengths to transition probabilities their experimental value is quite close to what is being deduced from VIRTIS (personal communication). The HITRAN value for the line intensities of the 0-1 are based on a non-observation of the 0-1 band from which a ratio 1/10 for the ratio of 0-1/0-0 intensities was inferred. Thus, the VIRTIS findings could be incorporated into the HITRAN database. For the Earth a recommended value for the transition probability of 52 ± 15 is given in Winick, et al., 1985. At the moment there is no evidence of variability or local dependence of the ratio in our data but this point has to be further confirmed by a more extensive study.

The O2 emission rate from nadir observations

The nightside spectra of Venus in the near IR spectral range from 1 to 5 μm (IR spectral channel of VIRTIS) are composed by the thermal emission of the lower atmosphere coming through the windows between the CO_2 absorption bands and scattered by the clouds, by the thermal emission of the clouds and the atmosphere above the clouds, prevailing at wavelengths longer than 3 μm and by the night airglow emissions. Among the latter ones the most pronounced is the O_2 at 1.27 μm. It overlaps with the thermal emission at about the same wavelength. However the maximum of the O_2 emission is shifted to the short wavelengths compared to the maximum of the thermal emission. Despite the relatively low spectral resolution of VIRTIS-M, which doesn't allow to spectrally resolve the two, we can visually identify the areas caused by the O_2 airglow on the disk by plotting an RGB image, using three spectral bands in the window. The areas of the O_2 emission will look bluish or white, comparing to the surrounding, see example of Fig. 1.

In the case of limb view observations, the O_2 airglow and the thermal emission scattered by the clouds can be easily identified and the oxygen airglow becomes dominant at altitude higher than 90 km. This is not true for nadir observations and an evaluation of the thermal emission can be empirically done using an average of the spectra in the disk, almost free of O_2 airglow. The error is connected with the variation of intensity over the disk, however the contrast at 1.27 μm is small, because the single scattering albedo of the clouds is very close to 1 and the expected error is only a few percent. This can be seen in Fig. 1 where we see a low residual intensity of background and absence of clouds signatures in the area where the airglow becomes significant.

Another way to correct the thermal radiation at 1.27 μm is from a theoretical estimation of the thermal emission of the atmosphere starting from the observed spectrum in other windows, like 1.18 μm and then extracting the theoretical value at 1.27 μm. For different aerosol models for low and middle latitudes, where we usually observe the O_2 emission, and taking into account reasonable opacities and the theoretical value of ratio of the thermal emission, the 1.74 μm window is not reasonable to use because the contrasts in this window is much higher than at 1.27 μm.

In the study that we present here we consider the intensity at 1.18 μm from the experimental data and rescale thermal emission at 1.27μm with a factor variable from 0.27 to 0.38 evaluated from the region of the Venus disk almost free of airglow (the lowest intensity of the 1.27 um uncorrelated from the 1.18 um, by means of a scatter plot) and after that we extract thermal emission from the total 1.27 µm profile, resulting in a net airglow.

Some cases in nadir view geometry of airglow are shown in Fig. 10. Scale bar represents the vertical emission rate of the oxygen at 1.27 um and it is corrected by thermal emission, emergence angle and clouds backscattering as from Crisp et al., 1996.

It is known that the regions of high emission rate are associated with the stronger downwelling and that they typically appear in the anti-solar point region with significant local and temporal variability. Notwithstanding the significant variability observed for the brightness of the oxygen airglow over the planet, its local distribution does not seem random and as a matter of fact it shows very structured features, often recurrent, with very defined geometrical shapes. A frequent shape being observed in the emission is of the form of very elongated channels sometimes ending with a sort of a bubble, see panel a of fig. 10. Their appearance looks very similar to jets following specific path flows, with an extension from 1700 to 2300 km. Although the emission is related to vertical flow rather than to horizontal motion, however the oxygen responsible of the features seen in emission because of the downwelling, is transported by this horizontal motion and in this sense the appearance of the emission does contain information of how the source has been transported, at least where the collision starts to work and allows to see its effect in emission (when oxygen is below 105 km).

Others typical patterns being observed in nadir, and visible also in Fig. 10, are circular shape feature having no airglow emission inside in contrast with high emission in the proximity of the border and beyond, see the dark patch in panel e of fig. 10, diameter extension is about 800 km. It can be said simply that the atomic oxygen in this specific case is not transported by the horizontal motion into the circular pattern but the net boundary and the particular geometrical shape bring to think about a large upwelling region due to a convective bubble, or large thermal anomaly of unknown cause that inhibits the subsidence and associated downwelling, with no or very little atomic oxygen collisions and consequent absence of airglow emission. It is interesting to note that if we select the image corresponding to the thermal brightness (TB) at 4.2 um, as shown in panel f of fig. 10, the dark circular feature seen at the airglow band in panel e is quite well reproduced in panel f, meaning that this zone has got a TB lower than the surrounding. By radiative transfer calculation, the wavelength at 4.2 um probes in the altitude range from about 88 to 92 km which is the lowest extreme of the vertical emission of airglow. The TB of the dark patch is about 182 K, in contrast with the surrounding at 185 K. Despite the temperature retrieval is not formally done, we have evaluated that the difference is significant and it corresponds to a similar gradient for the actual atmospheric temperature in the mentioned layer. This is a further confirmation that the dark circular feature in TB may be induced by adiabatic cooling produced by upwelling flow able to inhibit the oxygen recombination (no downwelling) and subsequent suppression of emission (dark region in airglow). However, also gravity waves may be responsible of a similar behavior. Consistent with the interpretation is the whiter region in the top side of panel f where the TB is about 189 K. This region, which is the highest in TB, appears where the downwelling is maximum and then the oxygen airglow emission is brightest (see correspondent zone of panel e).

A more detailed study of the apparent motion of oxygen airglow in nadir view is discussed in another paper of this issue (Hueso et al., 2008).

Conclusion

A study of Venus oxygen nightglow from a limb geometry and also with some cases in nadir has been conducted with the VIRTIS instrument on board Venus Express. Data analysed have been taken in the period February - April 2007, all with an exposure time of 8 sec, high enough to have a good SNR in the 1 to 3 μm spectral region.

All data have been acquired with almost the same local time, at about midnight to 01h; latitude coverage is 10-70 deg in the northern hemisphere. For the moment this does not allow to identify a dependence of the oxygen nightglow with time, if present, but a possible dependence of airglow intensity with latitude. The limb measurements of VIRTIS allow to retrieve the vertical profiles of the O_2. The shape of the vertical profile, its width and peak altitude are highly variable. Despite all, some regularities can be identified, especially at short term. The emission profiles with single peak usually owns a maximum at 97±1 km and for this case the intensity of emission decreases while peak altitude increases with increasing latitude. Often the second peak appears at altitudes in the range 103-105 km. High altitude of emission, vertical profiles with two maxima may have the cause in a higher wave activity. The highest value of emission rate for the considered set of orbits was found at low latitudes when peak of emission is at altitude higher than 100 km.

The 1.58 μm O_2 emission has also been measured in the VIRTIS spectra. Its vertical profile coincides with the vertical profile at 1.27 μm. The 1.27 μm/1.58 μm oxygen bands ratio have been measured and it results in a mean value of 77.9 ± 8.7 (63±6 for the ratio of the transition probabilities A_{00}/A_{01}).

Many others limb-like observations have been acquired by VIRTIS and not yet analyzed, and more are planned to be acquired in the incoming months. The other data will be included in the statistic and the airglow evolution with time will be also investigated.

Acknowledgements

We gratefully acknowledge the work of the entire Venus Express team that allowed these data to be obtained. We wish to thank ASI, CNES and the other national space agencies that have supported this research.

References

Bougher, S. W.; Borucki, W. J., Venus O2 visible and IR nightglow: Implications for lower thermosphere dynamics and chemistry. JGR, 99, p. 3759-3776 (1994).

Connes, P. Noxon, J. F. Traub, W.A. Carleton, N. O2/1 Delta/ emission in the day and night airglow of Venus. *Astrophysical Journal Letters*, **233**, L29-L32 (1979).

Crisp, D., Meadows, V.S., Bézard, B., de Bergh, C., Maillard, J.-P., Mills, F. P., 1996, Ground-based near-infrared observations of the Venus nightside: 1.27 um O2(a Delta g) airglow from the upper atmosphere, JGR, 101, E2, p. 4577-4594. (1996).

Drossart, P., Piccioni, G., Gérard, J. C., Lopez-Valverde, M. A., Sanchez-Lavega, A., Zasova, L., Hueso, R., Taylor, F. W., Bézard, B., et al., A dynamic upper atmosphere of Venus as revealed by VIRTIS on Venus Express, Nature, 450, p. 641-645 (2007). (Drossart et al., Nature 2007)

Drossart, P., Piccioni, G., Adriani, A., Angrilli, F., Arnold, G., Baines, K.H., et al., Scientific goals for the observation of Venus by VIRTIS on ESA/Venus express mission, P&SS, Vol 55, Issue 12, p. 1653-1672. (2007)

Drossart, P., Piccioni, G., Gerard, J.C., Lopez-Valverde, M.A., Sanchez-Lavega, A., Zasova, L., Hueso, R., Taylor, F., Bezard, B., Adriani, A., Angrilli, F., Arnold G., Baines, K.H., Bellucci, G., Benkhoff, J., Bibring, J.P., Blanco, A., Blecka, M. I., Carlson, R.W., Coradini, A., Di Lellis, A., Encrenaz, T., Erard, S., Fonti, S., Formisano, V., Fouchet, T., Garcia, R., Haus, R., Helbert, J., Ignatiev, N.I., Irwin, P., Langevin, Y., Lebonnois, S., Luz, D., Marinangeli, L., Orofino, V., Rodin, A.V., Roos-Serote, M. C., Saggin, B., Stam, D. M., Titov, D., Visconti, G., Zambelli, M., Tsang, C., & the VIRTIS-Venus Express Technical Team. Venus upper atmospheric emissions from VIRTIS spectral imaging observations. Nature, 29 November, 2007

Fox, J.L., and Borucki, S.W., Structure, luminosity and dynamics of the Venus thermosphere, Space Sci. Rev., 55, p. 357-489. (1991)

Gérard, J.-C.; Saglam, A.; Piccioni, G.; Drossart, P.; Cox, C.; Erard, S.; Hueso, R.; Sánchez-Lavega, A, Distribution of the O_2 infrared nightglow observed with VIRTIS on board Venus Express, Geophysical Research Letters, Volume 35, Issue 2 2008

Goldstein, J., Absolute wind speed measurements in the low atmosphere of Venus using infrared heterodyne spectroscopy, PhD thesis, Univ. of Penn, 1989.

(Hueso et al, JGR this issue)

Ohtsuki, S., N. Iwagami, H. Sagawa, H. Kasaba, Y. Ueno, and M. Imamura, Groundbased observation of the Venus 1.27-mm O2 airglow, Adv. Space, 36, 2038. (2005).

Ohtsuki, S., Iwagami, N., Sagawa, H, et al., Imaging spectroscopy of the venus 1.27-µm O_2 airglow with ground-based telescopes, Submitted to Adv. Space Res., ??

Piccioni, G. et al. VIRTIS: the Visible and Infrared Thermal Imaging Spectrometer (ESA-SP-1295, ESA Publications Division, Noordwijk, The Netherlands, in press.

Rothman L.S., et al., 'The HITRAN 2004 molecular spectroscopic database', Journal of Quantitative Spectroscopy & Radiative Transfer 96, p. 139–204, (2005).

Sharma, R. D., Harlow, H. B., Riehl, J. P., Determination of atomic oxygen density and temperature of the thermosphere by remote sensing, P&SS, 36, p. 531-538. (1985).

Slanger, T., D. L. Huestis, P. C. Cosby, N. J. Chanover, and T. A. Bida (2006), The Venus nightglow ground-based observations and chemical mechanisms, Icarus, 182, 1.

Titov, D.V., Svedhem, H. , Koschny, D., Hoofs, R., Barabash, S., Bertaux, J.-L., Drossart, P., Formisano, V., Häusler, B., Korablev, O., Markiewicz, W.J., Nevejans, D., Pätzold, M., Piccioni, G., Zhang, T.L., Merritt, D., Witasse, O., Zender, J., Accomazzo, A., Sweeney, M., Trillard, D., Janvier, M. and Clochet, A., Venus Express science planning, PSS, 54, p. 13-14. (2006)

Winick, J. R., Picard, R. H., Sharma, R. D., Nadile, R. M., Oxygen singlet Delta 1.58-micrometer (0-1) limb radiance in the upper stratosphere and lower mesosphere, JGR, 90, p. 9804-9814. (1985)

Yung, Y.L., and DeMore, W.B., Photochemestry of the stratosphere of Venus: Implications for atmospheric evolution, Icarus, 51, p. 199-247. (1982).

Figures and tables

Cube Name	Date (start of observation)	Lat (deg)	Long (deg)	Local Time (h)	Main peak Position (km)	FWHM (km)
Limb view geometry						
VI0076-18	2006-07-06T01:34:11.885	32-61	150-182	21.8-23.9		
VI0271-09	2007-01-17T07:36:25.808	15-35	355-35	23.8-2.4		
		15-20			98±1	
		20-25			98±1	
		30-35			98±1	
VI0275_06	2007-01-21T07:33:11.848	20-37	28-35	0.6-1.1		
		30-35			96±1	
VI0317-06	2007-03-04T06:12:02.628	13-33	163-169	00-01		10.4
		15-20			97±1	
		20-25			97±1	
		25-30			96±1	
VI0317-07	2007-03-04T06:26:02.647	25-42	167-169	0.2-0.4		11.2
		25-30			97±1	
		30-35			96±1	
		35-40			96±1	
		40-45			98±1	
VI0317-08	2007-03-04T06:40:02.683	49-75	170-131	0.5-0.9		8.5
		50-55			96±1	
		65-70			98±1	
VI0320-03	2007-03-07T06:09:36.553	13-33	167-173	01	93.5	8.6
VI0320-04	2007-03-07T06:23:36.563	25-47	172-131	0.4-0.5	95.5	7.8
VI0320-05	2007-03-07T06:37:36.463	48-75	174-135	1-1.3	92.8	9.7
VI0321-03	2007-03-08T06:08:48.557	13-34	168.5-175	0.8-1	92.2	9.5
VI0321-04	2007-03-08T06:22:48.581	28-50	173-175	0.7-1	94.0	12
VI0321-05	2007-03-08T06:36:48.600	47-75	176-135	1-1.3	98.7	14.7
		50-55			103±1	
VI0322-06	2007-03-09T06:07:58.719	13-31	170-176.5	0.7-1	93.1	8.5
VI0322-07	2007-03-09T06:21:58.548	26-49	175-176.5	0.7-1	96.5	7.7
VI0322-08	2007-03-09T06:35:58.735	48-74	177-140.5	1-1.4		11
		50-55			96±1 103±1 (2nd peak)	
VI0323-06	2007-03-10T06:07:10.491	13-34	172-178	0.9-1.1	94.5	10.2
VI0323-07	2007-03-10T06:21:10.436	25-46	176-178	0.7-0.8	98.1	10.7
		35-40			100±1	
		40-45			101±1	
VI0323-08	2007-03-10T06:35:10.636	48-75	179-142	1-1.6	96.7	10.4
		50-55			101±1	
VI0324-06	2007-03-11T06:06:22.643	12-32	173-179	1-1.5	96.4	
		15-20			101±1	
VI0324-07	2007-03-11T06:20:22.675	25-45.5	178-179	1-1.2	95	
		25-30			99±1	
VI0324-08	2007-03-11T06:34:22.812	48-74	180-143	1-3.5	97.5	
		65-70			97±1	
VI0327-05	2007-03-14T06:03:57.657	12.5-33	177-183	1.5-1.8	95.6	

		15-20			102±1	
VI0327-06	2007-03-14T06:17:56.638	25-47	182-183	1.4-1.5	92.7	
VI0327-07	2007-03-14T06:31:57.562	48-75	185-147	1.3-4	95.6	
VI0330-04	2007-03-17T06:01:32.677	12.7-32	182-188	1.8-2.1	92.4	
VI0330-05	2007-03-17T06:15:32.526	25-48	187-188	1.7-1.8	92.9	
VI0330-06	2007-03-17T06:29:32.724	47-75	189-150	1.7-4.3	96.1	
VI0364_08	2007-04-21T02:01:58.319	27- 46	345- 355	22		
		35-40			99±1	
VI0371_10	2007-04-27T05:42:01.476	25-60	354-2.2	22.6-23.1		
		35-40			99±1	
VI0377_11	2007-05-03T05:37:23.428	24-58	1.1-10.9	23.2-23.9		
		45-50			100±1	
		50-55			101±1	
VI0443_06	2007-07-08T07:36:05.904	-3.9-17	160-189	0.9-2.9		
		10-15			99±1	
Nadir view geometry						
VI0044-01	2006-06-03T15:06:56.666	-79- -10	9- 119	3- 19		
VI0093-00	2006-07-22T15:00:09.506	-2- -59	130-182	1.3-4.7		
VI0093-01	2006-07-22T15:28:09.436	7- -61	178-246	20.9-1.5		
VI0093-02	2006-07-22T15:56:09.547	11.3- -45.2	218-272	19-22.8		
VI0574-05	2007-11-15T18:42:55.387	15.7- -40	0	16		
VI0264-04	2007-01-09T20:36:56.857	-11- -78	75-323	20-3		
VI0344-01	2007-03-30T23:32:32.912	-	-	-		
VI0574-05	2007-11-15T18:42:55.387	-40- 16	0	16		
VI0586-01	2007-11-27T16:53:15.434	-62- 9	0	19		

Table 1. Summary of selected data. The covered period is from July 2006 to march 2007. In the case of limb observations, the peak altitude is given for a 5 deg latitude range and FWHM is also shown as a mean value for the considered session.

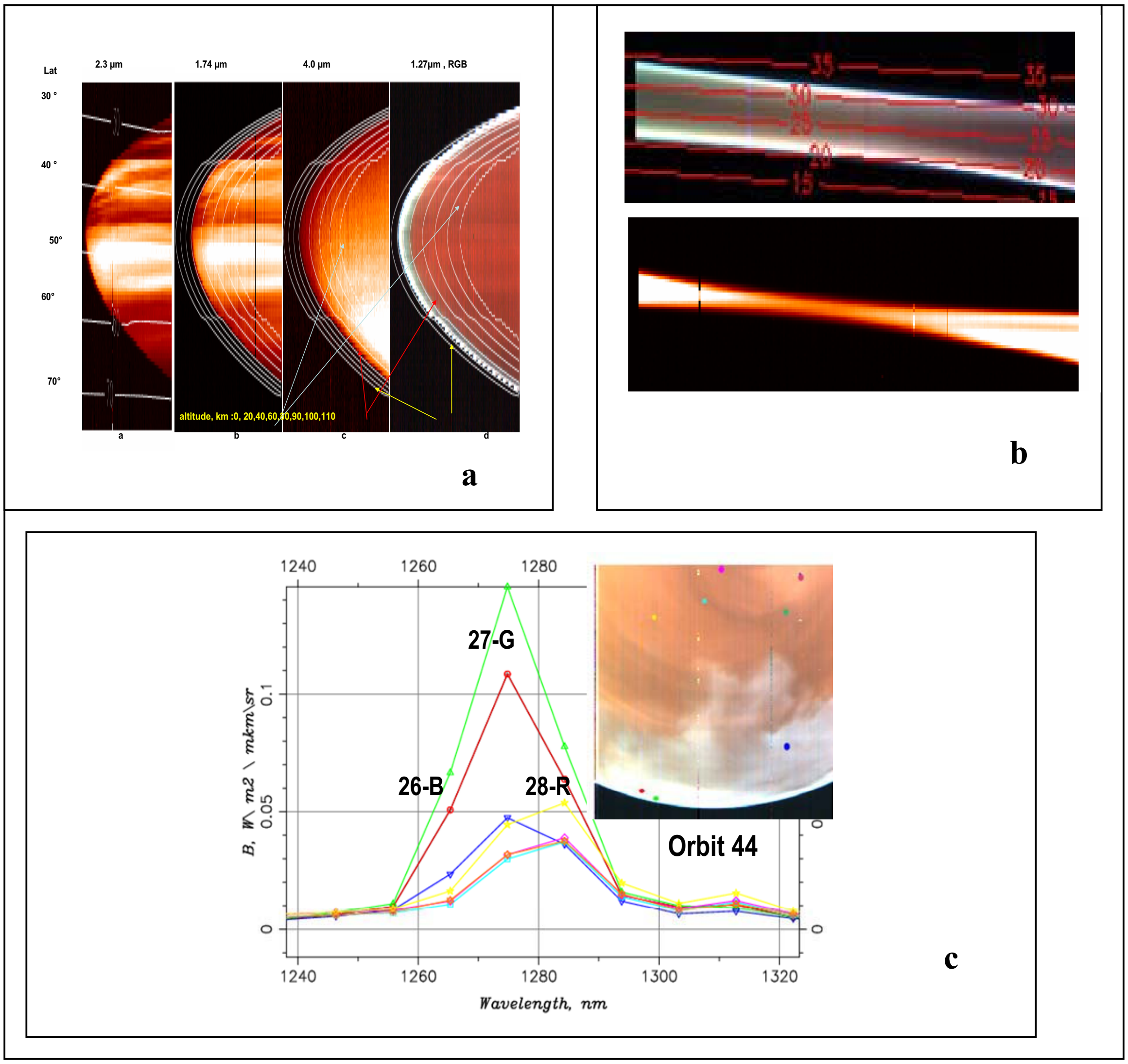

Fig.1 a). Orbit 76_18 in limb tangential mode. The RGB image in the 1.27 µm window, the images in 2.3µm (thermal emission of the lower atmosphere scattered by the clouds), and thermal emission of clouds at 4µm are shown. Thermal emission is extended up to the altitudes exceeding 80 km.

b) Orbit 271_09 in limb inertial mode. RGB image at 1.27 µm (latitudes are given in figure and image at 1.74 µm at the same scale

c) Nadir observations, orbit 44. Spectra in the 1.27 µm window. Colors of spectra coincide with color of area on the RGB image. Positions of the R,G and B bands are shown on the spectra. The area of O_2 emission has white color. It can be seen the shift of the airglow maximum emission in spectra from the thermal emission of the clouds (to compare green and magenta spectra).

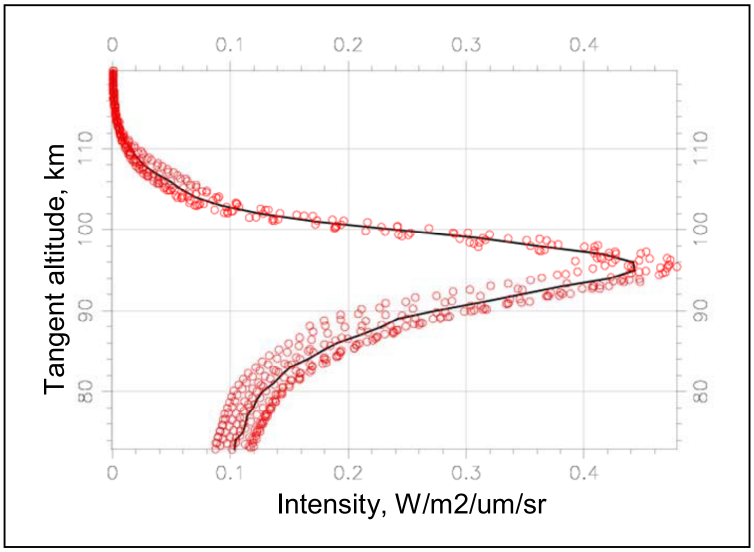

Fig. 2. Example of the limb vertical profile, Y-axis is tangent altitude. Orbit 316_06, φ=15-20°N. All pixels within this latitude range are shown and (black) – vertical profile, obtained by smoothing within 1 km (spatial resolution of VIRTIS-M for this orbit is of 2 km).

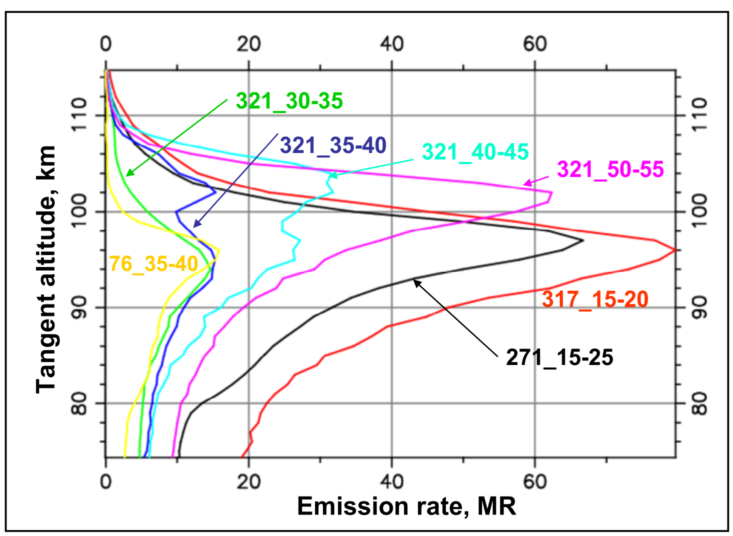

Fig.3. Emission rate for different orbits in limb profiles.

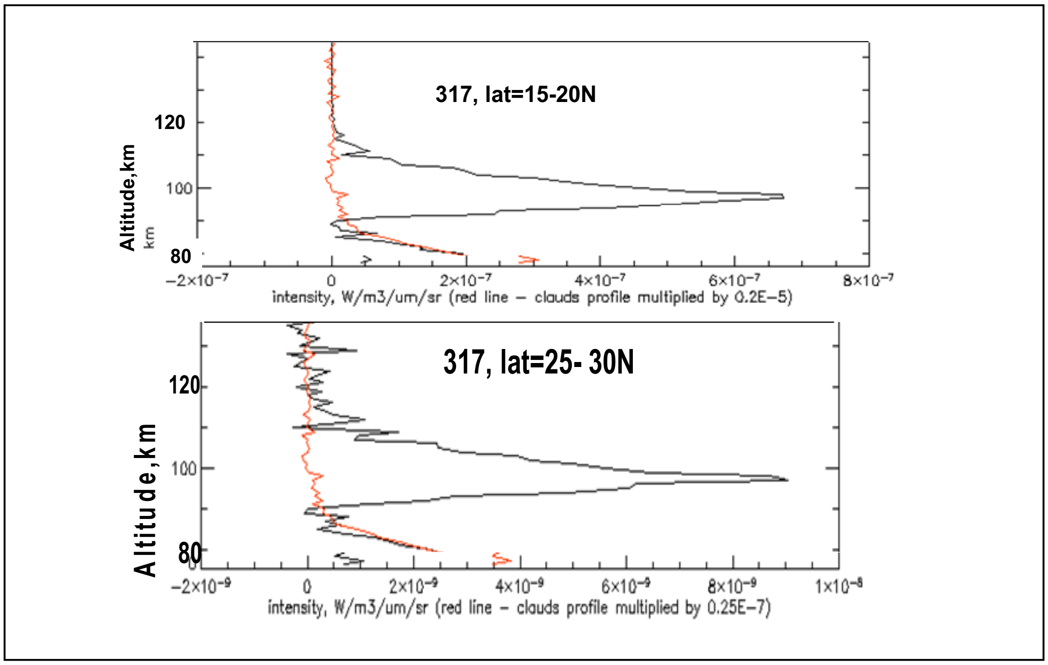

Fig. 4. Vertical profiles of volume emission, black – orbit 317_06 in 1.27 µm , red – normalized intensity at 1.74 µm, which describes upper boundary of clouds. For both plots normalized vertical profile of thermal emission in 1.74 µm coincides well with the retrieved emission in the 1.27µm, which is also thermal emission of the clouds.

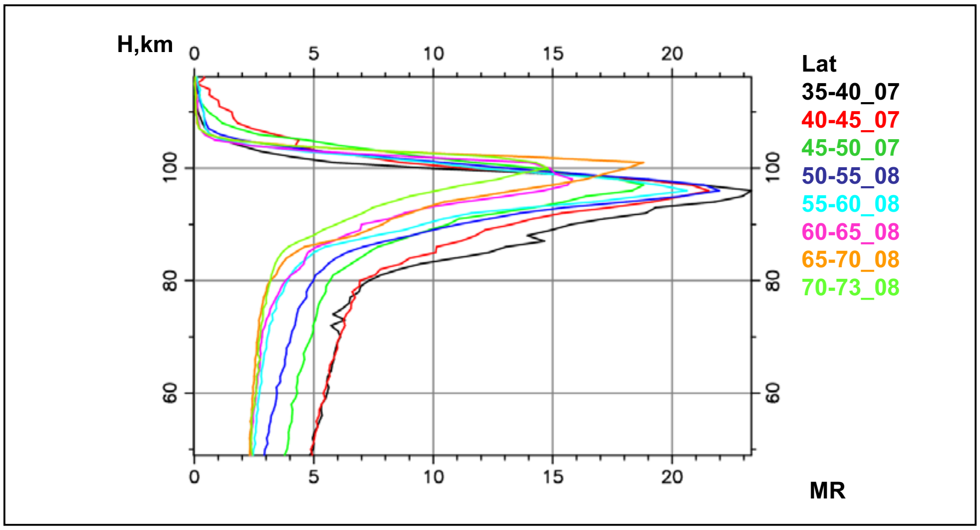

Fig.5. Limb profiles for orbit 317 from 35 to 73 °N

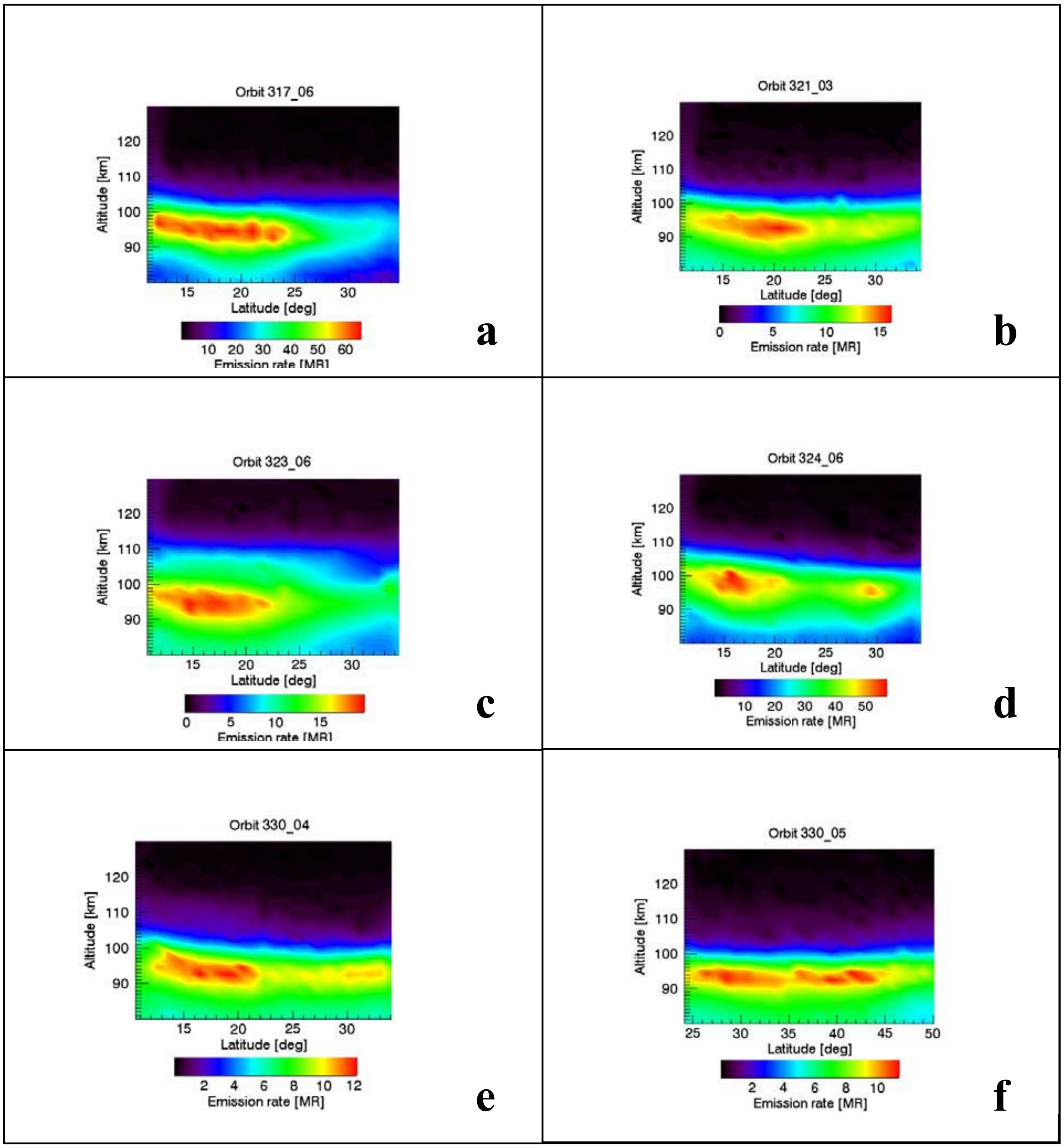

Fig. 6 Vertical distribution of the oxygen airglow at 1.27 um versus latitude. The intensity is integrated over all the local time at the same latitude. The color bar is the emission rate along the line of sight. The orbit and session number are given in the titles of the panels. The emission rate can be significantly different from one limb to another one, see for example the comparison of the panel a and b. Within the same orbit, regular trends are observed for the altitude versus latitude. The altitude can be almost constant like panel f or more frequently a slope is observed like the other panels. Some small features "wave-like" as in panel b at 27 deg latitude are real and may be attributed to gravity waves.

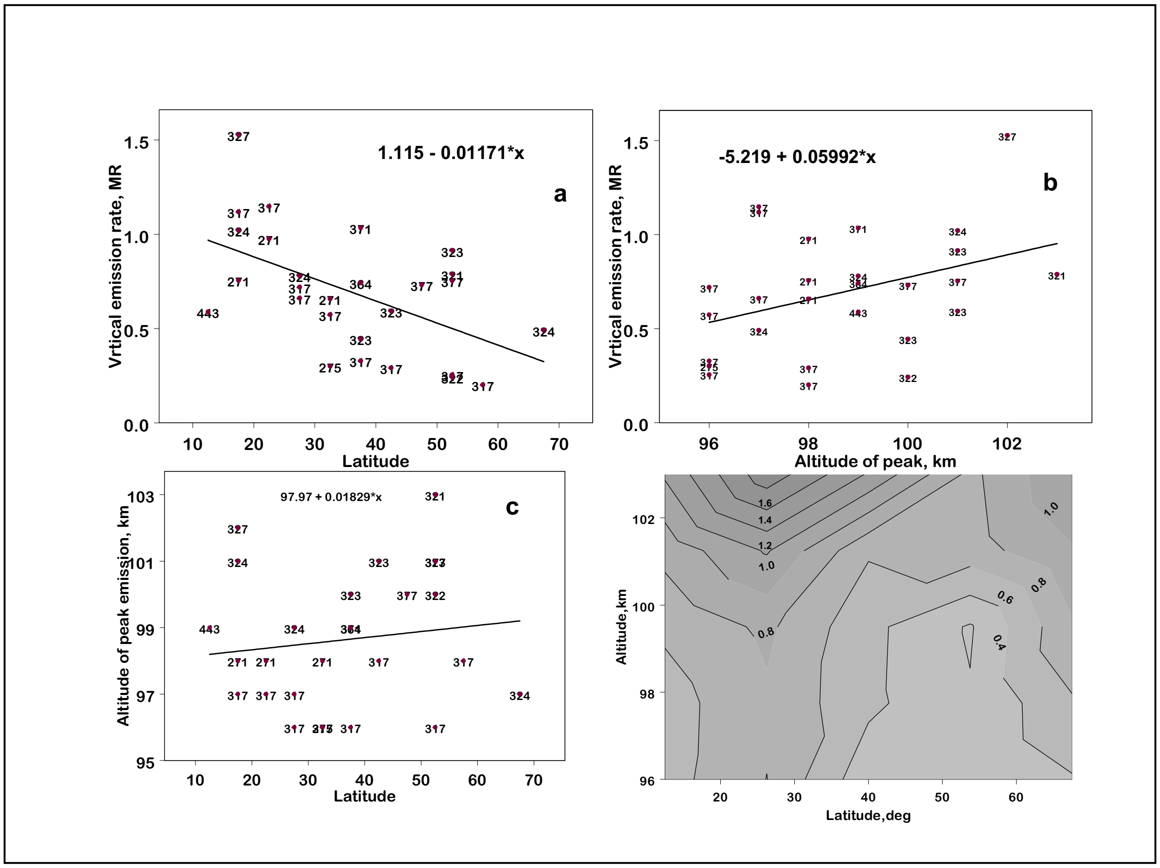

Fig.7. a) Vertical emission rate vs. latitude, points are marked by numbers of corresponding orbit, line is a linear least square fit of the data; b) same as a) but vs. altitude of peak; c) same as a) but altitude of peak emission vs. latitude; d) vertical emission rate (MR) vs. the peak altitude and latitude

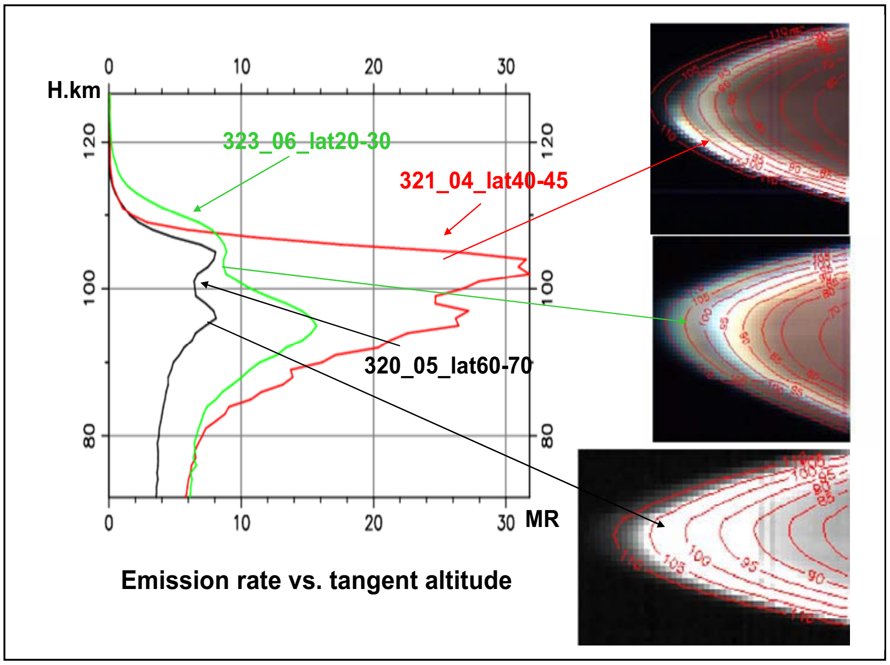

Fig. 8 . Examples of limb profiles with two maxima of intensity.

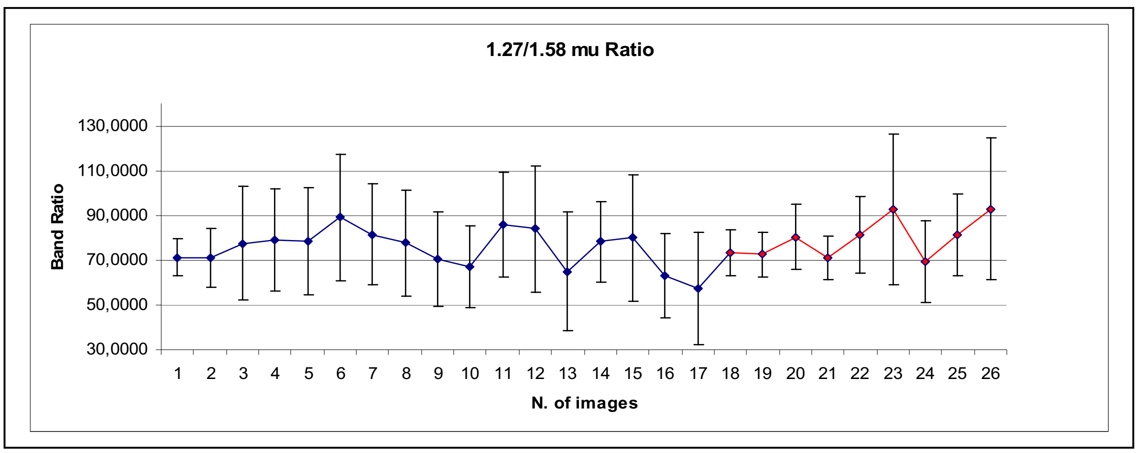

Fig. 9 1.27 µm/1.58 µm oxygen bands ratio. The statistic takes in account all the data analyzed, in the period Feb-Apr 2007. The weighted mean value is 77.9 ± 8.7

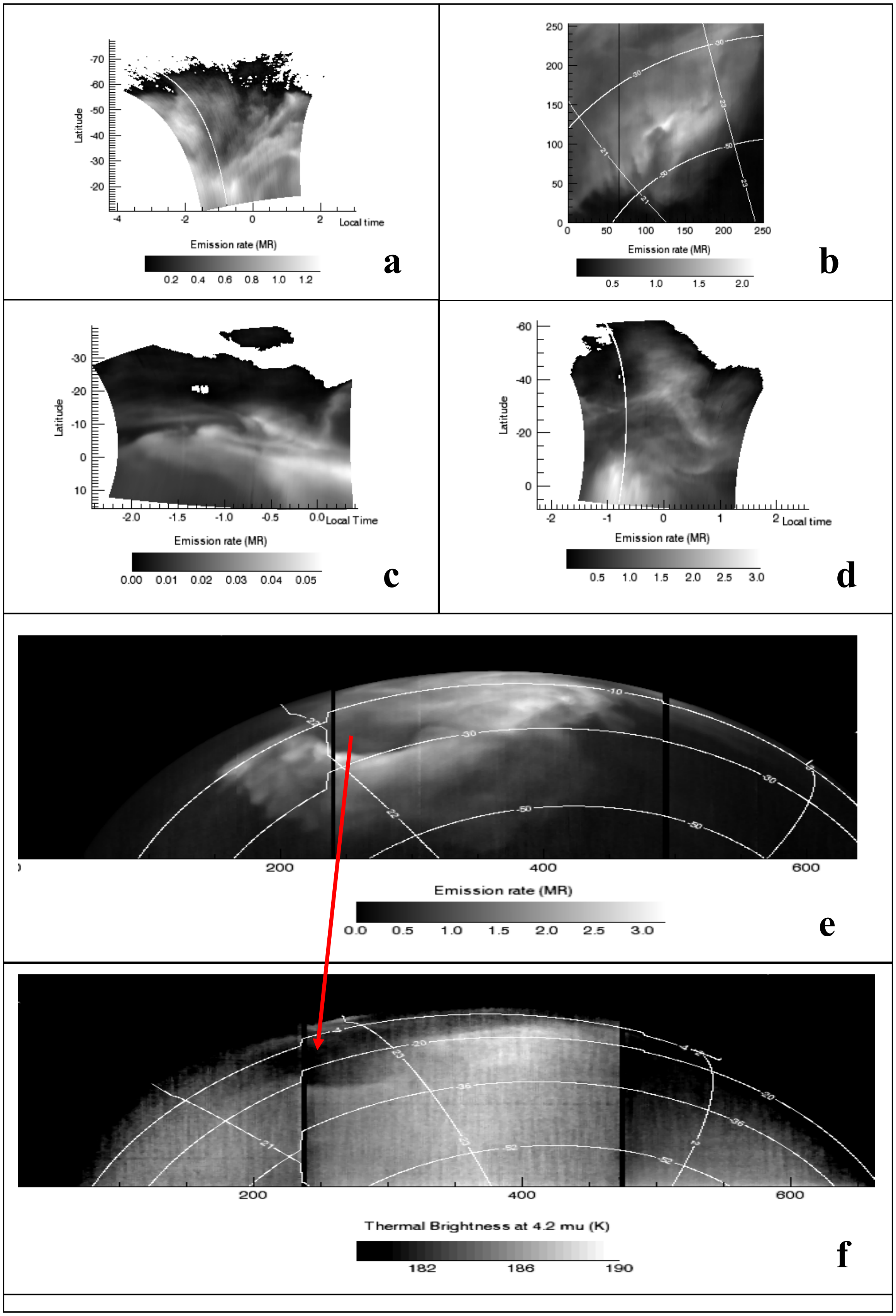

Fig. 10 Observations in nadir view geometry.

a,b,c,d,e are airglow observations at 1.27 um band, after thermal and emission angle corrections. f is the thermal brightness at 4.2 um from the same cube as from e.

a) orbit 264 session 04. b) orbit 344 session 01. c) orbit 574 session 05. d) orbit 586 session 01. e) orbit 93, mosaic of session 00, 01 and 02. f) orbit 93 session 01.

The extension of the long stripes in panel a is of the order of 1700-2300 km.

For the observation in panel f, the thermal brightness at 4.2 um, according to the radiative transfer calculations, is related to the temperature of the layer at about 88-92 km altitude. Despite this layer is the lowest interested by the vertical profile of the airglow, the TB of the dark patch indicated by the arrow is about 182 K, which is 3 K lower than the surrounding. This is visibly correlated with the correspondent dark patch in panel e of oxygen airglow. The diagonal dimension of the dark circular feature is about 800 km. The whiter region in the top center has got the higher TB of the image, about 189 K which is consistent with the maximum downwelling zone.